Article

Outdoor Thermal Environments of Main Types of Urban Areas during Summer: A Field Study in Wuhan, China

Kun Li *[ORCID]**, Xuefei Li and Keji Yao**

School of Urban Design, Wuhan University, Wuhan 430072, China; Li1018@whu.edu.cn (X.L.);
yaokeji@whu.edu.cn (K.Y.)
* Correspondence: kunli@whu.edu.cn

Abstract: Under the influence of the urban heat island effect, the thermal environments of urban built-up areas are poor, leading to the loss of urban vitality and the extreme deterioration of thermal comfort. In this paper, the outdoor thermal environment in Wuhan's main urban area is studied via the use of field measurements. From June to August in the years 2015 to 2017, 20 measurement points were selected for monitoring from 08:00 to 19:00 h, which were located in spaces such as residential areas, parklands, commercial streets, and college/university campuses. The measurements for the same types of land and different types of land use are analyzed. A comprehensive thermal environment index is used to quantitatively evaluate the overall situations of thermal environments. The results showed that the cooling effect of vegetation shading was stronger than the effect of water evaporation and the maximum temperature difference between the two cooling methods reached 6.1 °C. The cooling effect of the canopy shading of tall trees was stronger than the effect of grassland transpiration and the maximum temperature difference was 2.8 °C. The streets with higher aspect ratios might improve the ventilation, but the wind speeds remained low, which did not provide a strong cooling effect. This study helps urban planners understand the thermal environment of Wuhan or similar cities with hot summer and diversified urban areas, and puts forward suggestions to reduce the heat island effect from the aspect of building layout, green coverage, shading mode, and street aspect ratio, so as to establish sustainable cities that are climate adaptable and environmentally friendly.

Keywords: outdoor thermal environment; main urban area of Wuhan; field measurements; physiologically equivalent temperature

1. Introduction

Currently, more than half of the world's population lives in urban areas, and this proportion is expected to rise to 66% by 2050 [1]. Increasing urban populations and expanding urban areas have brought about a series of environmental consequences, such as hotter cities, global warming [2–4], more difficulty for people to participate in outdoor activities [5], increased urban resource consumption [6,7], storms and precipitation events [8], increased heat-related mortality [9,10], and high levels of urban pollution [11].

Some studies have shown that unreasonable layouts of the urban underlying surface, intensive human activities, and growing numbers of construction projects are all important factors contributing to the heat island effect [12–14]. Today, building materials consist mainly of reinforced concrete, which has the characteristics of lower heat capacity, faster heat absorption, and better storage temperature. This type of concrete is the main source of the heat that raises ground temperatures [15]. With the expansion of constructions, the reduced number of trees leads to a decrease in vegetation transpiration and less arbor canopy shade while the reduction in the surface areas of water bodies also exacerbates the heat island effect [16,17].

To help urban residents better adapt to the possible impacts of global warming and urban heat islands in urban thermal environments, as well as to improve the thermal

comfort of open urban spaces, scholars have adopted different methods to study outdoor thermal environments. Some studies have used field surveys and questionnaires. Yan et al. used measurement methods to analyze the thermal performance of a large urban vegetation park in Beijing and its impact on the surrounding urban thermal environment [18]. Yang et al. demonstrated through outdoor measurements that shade and trees could improve outdoor thermal environments [19]. Coutts et al. measured three streets running east to west under high-temperature weather in Melbourne, Australia, and found that the temperatures under tree canopies were lower and the minimum temperature could be reduced by 1.5 °C [20]. Tania Sharmin et al. used field measurements and questionnaires to analyze the outdoor thermal environment of Dhaka, a tropical city, and showed that urban geometry had a significant effect on urban microclimates and outdoor thermal comfort [21].

To study the influence of a certain factor on an outdoor thermal environment, some scholars have established scale models to be used outdoors or indoors. For example, Park et al. conducted field measurements on a scale model site to study the impact of urban vegetation on the outdoor thermal environment [22] and the impacts of different water forms (in the form of artificial ponds) on the urban thermal environment [23]. Du et al. combined wind tunnel testing and on-site monitoring, and then proposed strategies for designs to improve the wind environment and thermal comfort at the pedestrian height [24]. Janssen et al. used the computational fluid dynamics (CFD) model to study the wind comfort of pedestrians around a building and obtained very different conclusions on wind comfort according to different standards [25]. Jianlin Liu et al. combined the wind speed distribution simulated by a CFD model with air temperature, radiation temperature, and humidity field measurements and studied the effect of elevated design on the thermal comfort of the surroundings [26].

Ali-Toudert et al. evaluated outdoor thermal comfort with ENVI-met software [27]. Dwivedi et al. also used this software to simulate the thermal environment of the Mumbai metropolitan area, and then proposed the use of vertical walls and dense urban vertical coverage or forests to reduce the urban heat island effect [28]. Qaid et al. used ENVI-met software to simulate the study area for analyzing the thermal comfort of different hot spots in Putrajaya, Malaysia, and obtain wind speeds and building heights, which are the key variables for reducing the physiologically equivalent temperature (PET) thermal index [29].

In this study, Wuhan's representative urban spaces (high-density commercial streets, residential areas, college/university campuses, and urban green spaces, such as parklands) are selected for measurements during the summertime. The instruments, such as ultrasonic anemometer, temperature and humidity recorder and Black globe thermometer, are used. The indices of the summer microclimates of these typical urban spaces in Wuhan, such as air temperature, relative humidity, wind speed and direction, are obtained. The research focuses on high-temperature processes. The spatial structures of these land types are relatively homogeneous and simple. The environmental conditions of similar areas can be determined from the case points.

Then, a quantitative analysis was put forward in terms of vegetation planting, building aspect ratios, suitable water feature layouts, and reasonable shading. In the research, the shade of the building could reduce the temperature by 3.5 °C. Vegetations kept the thermal environment stable in summer. The temperature difference between the underlying surfaces of vegetation and water body could reach 6.1 °C. The temperature difference between the reasonable and unreasonable arrangements for outdoor public venue would reach about 6 °C. A street with an aspect ratio of 2 had higher wind speed, but its temperature was 2 °C higher than a street with an aspect ratio of 1. It showed wind speed in normal streets was low and had limited function of ventilation. From the PET value regression analysis, air temperature had greater influence than relative humidity and wind speed. According to these results, suggestions can be provided from the perspective of optimizing the thermal comfort of urban residents in urban environment.

2. Methodology

2.1. Study Area

Wuhan City (113°41′–115°05′ E, 29°58′–31°22′ N) is located in central China, east of the Jianghan Plain and the lower reaches of the Yangtze River. Wuhan's climate is subtropical humid with hot summers from June to September, where the maximum temperature can reach 39.4 °C [30]. Thermal environmental issues are very prominent in this area. The main urban area of Wuhan is selected as the study area, which is generally considered as the urban area within the third traffic ring. This area is also the place with the strongest heat island effect and poor thermal environment in Wuhan (Figure 1).
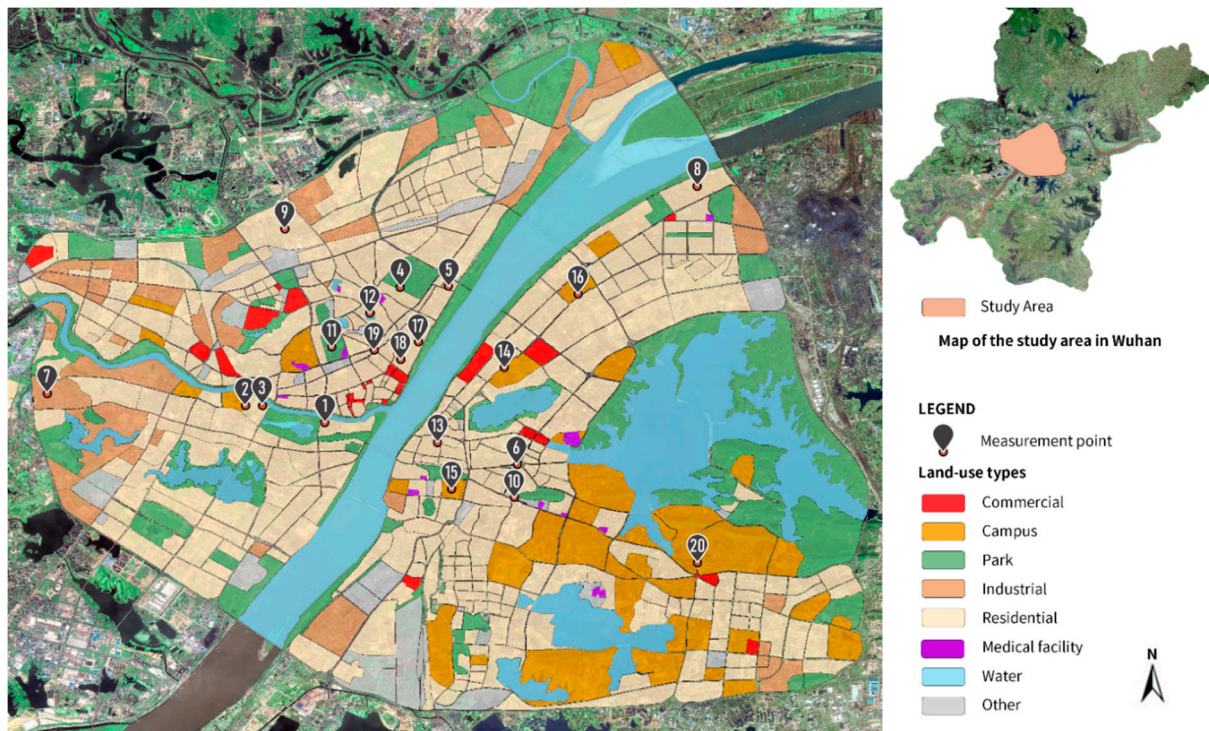

Figure 1. Distribution of measurement points.

Wuhan is a city with a population of 11.2 million in central China, with an urban area of 8569.15 km^2 [31]. The city contains different kinds of spaces and rich underlying surface types, such as residential districts with various densities, large rivers and lakes and commercial streets. The thermal environment of Wuhan is complex and has diversified unique characteristics.

2.2. Characteristics of Urban Spaces

This study was conducted in July and August 2015 to 2017. These two months are the summer in Wuhan and the hottest time of the year. This study selected 9 days out of all the observation days for all-weather outdoor thermal environment analysis and research, as shown in Table 1 [32]. The measured physical quantities included air temperature and relative humidity, as well as instantaneous wind speed and direction. A total of 67 measurement points were obtained and 20 were selected for analysis, which included residential land-use type (Points 1, 2, 3, 8, 9, and 17), urban park land-use type (Points 4, 6, 10, 11, and 12), commercial land-use type (Points 5, 13, 19, and 20), college/university campus land-use type (Points 14, 15, and 16), industrial land-use type (Point 7), and medical facility land-use type (Point 18). These measurement points are shown in Figure 1.

Table 1. Characteristics of the locations of the measurement points.

Number	Date of Measurement	Land-Use Type [1]	Building Height	Building Density	Green Coverage Ratio	Abbreviation
1	13 July 2015	R	Multistory	High	Low	R-MHL
2	13 July 2015	R	Multistory	Low	Medium	R-MLM
3	13 July 2015	R	High-rise	Low	Low	R-HLL
4	14 July 2015	G	/	/	High	G1
5	14 July 2015	B	Low-rise	High	High	B-LHH
6	17 July 2016	G	/	/	Medium	G2
7	17 July 2016	M	Multistory	High	Low	M-MHL
8	23 July 2016	R	Low-rise	Medium	Medium	R-LMM
9	23 July 2016	R	Multistory	High	Low	R-MHL
10	26 July 2016	G	/	/	High	G3
11	26 July 2016	G	/	/	High	G4
12	26 July 2016	G	/	/	High	G5
13	13 August 2016	B	Multistory	High	Medium	B-MHM
14	10 July 2017	C	Multistory	Medium	High	C-MMH
15	10 July 2017	C	Multistory	Medium	High	C-MMH
16	22 July 2017	C	Multistory	Medium	High	C-MMH
17	22 July 2017	R	Low-rise	High	Low	R-LHL
18	22 July 2017	H	High-rise	High	Medium	H-HHM
19	25 July 2017	B	Multistory	High	Low	B-MHL
20	25 July 2017	B	High-rise	High	Low	B-HHL

[1] C signifies campus land-use type; H signifies medical facility land-use type; B signifies commercial land-use type; G signifies park land-use type; M signifies industrial land-use type; and R signifies residential land-use type.

In Table 1, the types of land use were classified referring from the "Code for classification of urban land use and planning standards of development land" [33]. Building height refers to the average height of buildings in the area where the measurement point is located, which can be divided into three categories: low-rise buildings (1–3 F), multistory buildings (4–9 F), and high-rise buildings (≥10 F) [34]. As it is shown in Appendix A Table A1, green coverage ratio was divided into low (<30%), medium (30–60%), and high (>60%). Additionally, in Table A2 in Appendix A, building density was divided into low density (<15%), medium density (15–30%), and high density (>30%). The letters in the abbreviations represent the type of land use, building height, building density, and green coverage ratio, respectively.

These types occupied large proportions of the urban land in Wuhan, and each had different outdoor thermal environments. The selected points are representative, which can be used to analyze the thermal environment of the same type of urban space, and can also be used to compare the thermal environment of different land-use types. Three main types of residential buildings were studied: traditional residential buildings (Point 17 [35]), a multistory staff dormitory built in the 1990s (Points 1, 8 and 9), and newly built mid-to-high-rise residential buildings, which exhibited high-rise low-density urban forms (Points 2 and 3). City parks, such as Hongshan (Point 10), Zhongshan (Point 11), and Baodao Parks (Point 12), usually use large and complete green spaces that incorporate various types of plants and water bodies intended to improve the microclimates of the parks. Commercial streets included two types. The first type comprised linear spaces that were building-based, had low green coverage ratios, and had high degrees of ground hardening (Points 13, 19 and 20). This type was formed between commercial buildings and urban

roads. The other type was formed by two rows of multistory buildings and comprised strips of spaces with high greening coverage ratios and moderate building densities (Point 5). College/university campuses tend to be independent, complete ecosystems (Points 14, 15 and 16). The buildings are mainly multistory or high-rise. The overall building densities are low and the layouts are loose. The overall green coverage ratios are high, forming more pleasant microclimates, but the use of large-scale impermeable paving tends to have negative effects.

The measuring points were selected in the typical outdoor spaces in these areas, and the thermal environment structure was in a state of dynamic stability. That means the index of thermal comfort, such as temperature and relative humidity, may change with weather and time, but the thermal environment structure may keep stable. Therefore, the thermal environment at the location of the measuring point may be the representation of the same type of area when the surrounding building height, building density and green coverage are similar.

2.3. Thermal Environment Monitoring

The air temperatures, relative humidities (RH), wind speeds, and wind directions of the selected urban spaces were monitored for the objective evaluation of the thermal comfort levels of outdoor spaces. The base data (including hourly temperature, relative humidity, and wind speed) used for comparison were taken from the National Weather Station (30°21′36.00″ N, 114°1′48.00″ E) in Hannan District in the southwestern, suburban area of Wuhan.

To avoid possible sources of interference, the measuring instruments at each measurement point were placed more than 3 m away from a building (Figure 2). Pedestrians were prohibited from approaching or touching the instruments. The wind speed and direction recorder consisted of a probe and tripod. The height of the probe was set at about 1.8 m above the ground. The measuring instruments are shown in Figure 3. The accuracy of the wind speed measurement was ±0.3 m/s and the change was between −30 °C and 80 °C. The accuracy of the wind direction measurement was ±3° and the range was 0–360°. A TR-72wf recorder was placed in the middle of the tripod at about 1.5 m above the ground to measure the air temperature and relative humidity for 12 h. The instrument automatically recorded data once every minute from 08:00–19:00 h. The accuracy for temperature was ±0.5 °C and the range was between −30 °C and 80 °C. The accuracy for humidity was ±5% RH, which was converted to 0–99% RH. Each observation station operated continuously for three days from 08:00–19:00 h. The black globe thermometer was used to show the ambient radiant temperature [36]. Its accuracy was ±0.3 °C and the range was between −10 °C and 70 °C. Stable and continuous measurements were selected for unified processing.
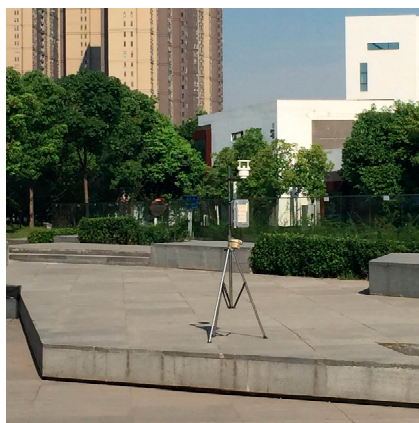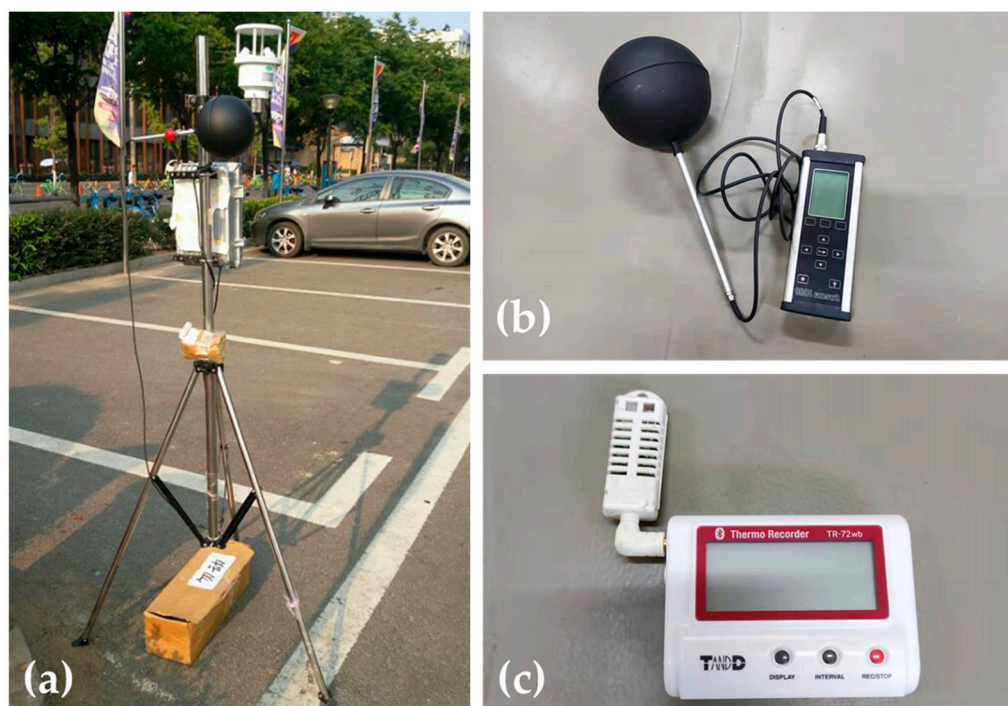

Figure 2. Field measurement photos.

Figure 3. Instruments used for the investigation. (**a**) Ultrasonic anemometer; (**b**) Black globe thermometer; (**c**) Temperature and humidity recorder (TR-72wf).

2.4. Daily Weather Conditions during Measurements

The meteorological conditions of the selected days are shown in Table 2. During the measurement period, the lowest temperature was 29.1 °C and the highest temperature was 38.2 °C. The highest relative humidity was 92% and the lowest relative humidity was 43%. The maximum wind speed was 6.0 m/s and the minimum wind speed was 0.4 m/s. The coolest day was 17 July 2016 with an average temperature of 31.9 °C, whereas the hottest day was 25 July 2017 with an average temperature of 37.4 °C. On 14 July 2015, the all-day wind speed was the lowest with an average wind speed of 1.2 m/s, whereas, on 23 July 2016, the all-day wind speed was the highest with an average wind speed of 4.4 m/s.

Table 2. Meteorological parameters on each observation day at Wuhan Station (30°21′36.00″ N, 114°1′48.00″ E).

Day	Air Temperature (°C)				Relative Humidity (%)				Wind Speed (m/s)			
	Min.	Max.	Mean	SD	Min.	Max.	Mean	SD	Min.	Max.	Mean	SD
13 July 2015	31.7	35.0	34.0	1.0	54.0	70.0	59.6	4.6	1.8	2.4	2.0	0.3
14 July 2015	29.1	35.3	32.8	2.4	51.0	92.0	69.1	14.0	0.4	2.1	1.2	0.5
17 July 2016	29.7	33.4	31.9	1.2	66.0	81.0	72.6	5.6	1.3	3.9	2.3	0.7
23 July 2016	32.7	35.4	34.3	0.9	53.0	60.0	56.0	2.4	3.8	5.1	4.4	0.5
26 July 2016	34.1	37.2	36.1	1.0	47.0	66.0	54.3	5.5	2.3	4.6	3.7	0.7
13 August 2016	34.2	37.0	36.1	1.0	50.0	66.0	55.8	5.0	0.6	3.6	2.1	0.8
10 July 2017	27.3	30.8	29.5	1.1	71.0	88.0	77.8	5.1	1.6	3.2	2.3	0.5
22 July 2017	34.2	37.8	36.8	1.2	43.0	61.0	49.2	5.4	1.8	3.7	2.6	0.6
25 July 2017	35.8	38.2	37.4	0.8	46.0	55.0	48.7	2.8	0.6	2.5	1.6	0.6

2.5. PET Calculations

The Physiological Equivalent Temperature (PET) is defined as the air temperature at which, in a typical setting (without wind and solar radiation), the heat budget of the human body is balanced with the same core and skin temperature as under the complex outdoor conditions to be assessed [37]. It is related to air temperature, wind speed, relative

humidity, and radiant temperature obtained by the black globe thermometer. Some typical measurement points were selected to analyze the PET index by RayMan 1.2 Software [38]. A mathematical model of the PET index and other meteorological parameters was established to reflect the comprehensive thermal environments of different surface features.

3. Results of Analysis

Different types of land use in the main urban area of Wuhan have different types of outdoor urban forms and thermal environment characteristics. In this paper, urban spaces were selected to examine the outdoor thermal environments and the factors affecting them were summarized. In order to ensure the effectiveness, all comparisons of measurement point conditions were carried out on the same day.

3.1. Characteristics of Thermal Environments of Residential Areas

Figure 4a–c shows measurement Point 1 (R-MHL) in a multistory residential area with high building density, small public spaces, and less vegetation. Point 2 (R-MLM) was in a residential area with both multistory and high-rise buildings, and Point 3 (R-HLL) was in a residential area with high-rise buildings and low building density. Small trees and shrubs were planted in the flower beds among the residences and the overall green coverage ratio was low.

(a)   (b)   (c)

(d)   (e)
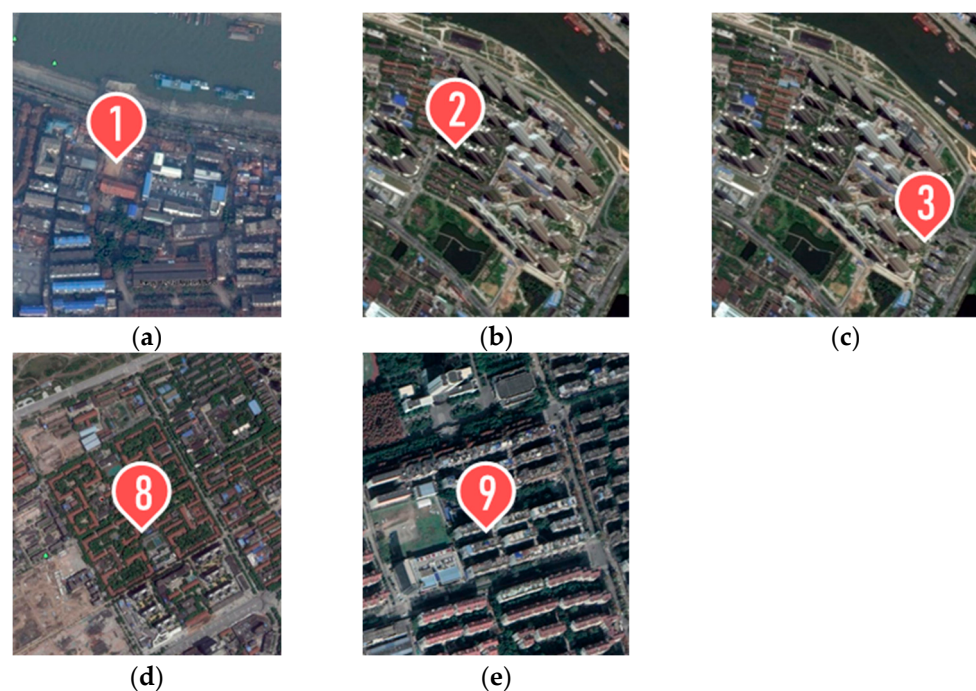
Figure 4. Satellite map of measurement points 1–3 and points 8–9. (**a**) Point 1; (**b**) Point 2; (**c**) Point 3; (**d**) Point 8; (**e**) Point 9.

The time average statistics of the above residential space measurement points during the daytime (09:00–17:59 h) on 17 July 2015 were conducted as shown in Figure 5. Before 12:00 h, the temperatures of Points 1 (R-MHL) and 2 (R-MLM) remained below 35 °C and 36.2 °C, respectively, whereas that of Point 3 (R-HLL) remained above 35.5 °C. As shown by the air temperature comparison in Figure 5a$_1$, the time of the maximum air temperature difference of the three measurement points was 09:00 h and the temperature of Point 3 (R-HLL) was about 3.5 °C higher than those of the other two measurement points. In the morning (before 12:00 h), Point 3 (R-HLL) was under direct sunlight, so the solar radiant heat caused the temperature to rise to 37.9 °C, whereas the other two measurement points lay in the shadow of the building and experienced the highest temperature at 36.1 °C. This result showed that the high-density dwellings around Point 1 (R-MHL) had formed a

zone of shadows that blocked the solar radiant heat and lowered the mean temperature to 34.4 °C, which was 1.2 °C and 2.3 °C lower than the daily mean temperatures of Points 2 (R-MLM) and 3 (R-HHL), respectively. However, the high building density and enclosed building layout at Point 1 caused the mean wind speed to be 0.4 m/s, whereas those at Points 2 (R-MLM) and 3 (R-HHL) were 0.8 m/s and 1.0 m/s, respectively. According to the above analysis, the effectiveness of breezes in reducing the air temperature was weaker than that of the shade. The temperature difference between the two forms of cooling was about 2 °C.
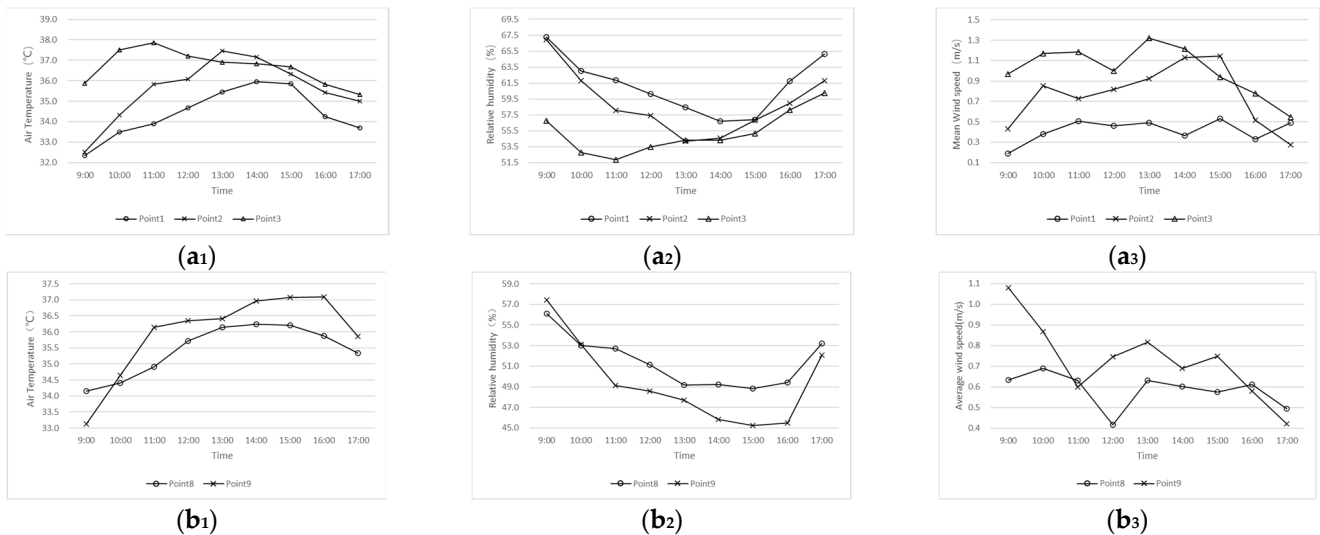
Figure 5. Comparison of measurement point parameters. (a_1) Temperature comparison; (a_2) Relative humidity comparison; (a_3) Wind speed comparison; (b_1) Temperature comparison; (b_2) Relative humidity comparison; (b_3) Wind speed comparison. The value on the abscissa axis represents the measurement hour. For example, 9:00 represents an hour within the range of 9:00–9:59, and the value on the ordinate axis represents the average value within each hour.

According to the above analysis, though solar radiation gradually increased in the morning, the enclosing buildings formed a zone of shadows that reduced the air temperature. In the shadow of the buildings, the temperature was 3.5 °C lower than that in direct sunlight, but the wind speed of this building layout was only 50% that of the buildings laid out in a row.

The measurements of Point 8 and Point 9 were made in another time period on 23 July 2016. Figure 4d,e shows Point 8 (R-LMM) beside the road of a multistory residential community. The buildings along both sides of the road were arranged to create an enclosure. Tall trees by the sidewalks close to this point provided good shade. Point 9 was located in the flower bed of a multistory residential area with high building density and a low greening rate. The buildings around the measurement point were arranged in a row. Figure 5b_1,b_2 shows that the temperature and wind speed at Point 8 (R-LMM) were lower than those at Point 9 (R-MHL). Between 09:00 and 11:00 h, the air temperature at Point 9 rose by 3 °C, whereas that at Point 8 increased by only 0.7 °C. As the shadow of the vegetation blocked the strong radiation of the sun, the temperature of the measurement point did not rise too rapidly, as shown in Figure 4d,e.

Figure 5b_1,b_2 shows that the all-day temperature at Point 8 (R-LMM) was lower than 36.2 °C, which was under severe high temperature [39], but the relative humidity was higher than that of Point 9 (R-MHL), which was under direct sunlight. The shade and transpiration of the trees at Point 8 increased the relative humidity and kept the temperature low so that the temperature difference in the daytime at Point 8 was within 2 °C. At Point 9, the temperature difference reached 4 °C in the daytime.

3.2. Characteristics of Thermal Environments of Urban Parklands

Figure 6a–c shows Points 10 (G3), 11 (G4), and 12 (G5) located in Hongshan Park, Zhongshan Park, and Baodao Park, respectively. Each park had high green coverage and was located on the hard pavement, but the combined types of the underlying surfaces were different. Point 10 was located on the hard pavement of the square at the park's entrance and had no shelter from the sun. This park was located in the central area of the city and the surrounding buildings were mainly multistory. The vegetation in the park consisted mostly of tall trees. Point 11 was located on the hard-paved square in the central area of its park and also had no shelter. The central area of the park had rich vegetation with tall trees creating dense shade and some water bodies, whose surface areas accounted for about 20% of the park's total area. Point 12 was located on the hard pavement of the island in the center of the park. The green coverage ratio of the island accounted for about 50% of the island's area while the surface area of the water bodies in the park accounted for about 62.5% of the park's total area.

(**a**)　　　　　　　　　　　　　　　　(**b**)　　　　　　　　　　　　　　　　(**c**)
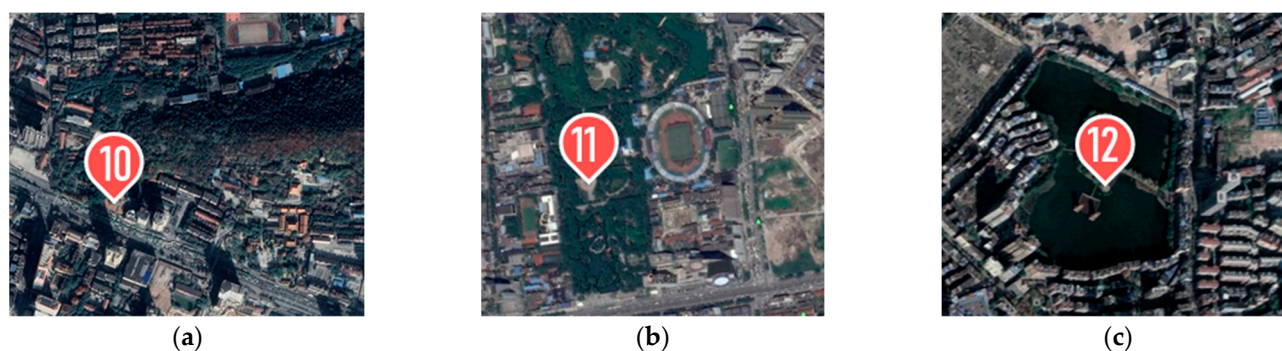
Figure 6. Satellite map of measurement points 10–12. (**a**) Point 10; (**b**) Point 11; (**c**) Point 12.

The average temperature of Point 12 was the highest, which was 2.8 °C higher than that of Point 10 and 4 °C higher than that of Point 11. Point 12 was surrounded by water, but the green coverage rate was about 50%, whereas the green coverage rates of Points 10 and 11 were as high as 90%.

The environmental characteristics of the three measuring points were found from the segmented intervals of time. Figure 7 shows that, before 11:00 h, the temperature at Point 12 (G3) was the highest (44.6 °C) and the increase was the greatest (12 °C within two hours), whereas the temperature at the other two points was the same at below 40.5 °C. All three measurement points were exposed directly to sunlight. The temperature at Point 12 was higher those at Points 10 (G3) and 11 (G4), indicating that the cooling effect of the water evaporation of Point 12's park was weaker than that of the high-density vegetation's transpiration in the other park. From 13:00 to 15:00 h, the average temperatures of Points 10, 11, and 12 were 43.2 °C, 40.4 °C, and 44.4 °C, respectively. Point 11 was covered by water and high-density vegetation. Under the joint action of water surface evaporation and vegetation transpiration, the temperature remained relatively stable. The wind speed also had a good cooling effect with the highest speed at Point 11. The wind speed at Point 10 was relatively high, but the temperature also rose significantly. Therefore, ventilation alone could not effectively alleviate the high temperatures during the summer afternoons.

From 15:00 to 17:00 h, the temperature dropped by 11 °C at Point 12 (G5) and by 3.07 °C at Point 10, but remained basically unchanged (dropped by 0.55 °C) at Point 11 (G4). When the intensity of the solar radiation gradually weakened, the temperature at Point 12 was drastically reduced by water evaporation, which performed better than the vegetation transpiration at Points 10 and 11. The maximum temperature difference between the two forms of cooling was 7.6 °C. At 17:00 h, the solar radiation was weak and the temperatures of both Points 10 and 11 on the hard-paved ground in the parks were still higher than 39.4 °C, whereas that of Point 12, which was on the island, dropped to 34.2 °C. The temperatures of Points 10 and 11 were 5.2 °C higher than that of Point 12.
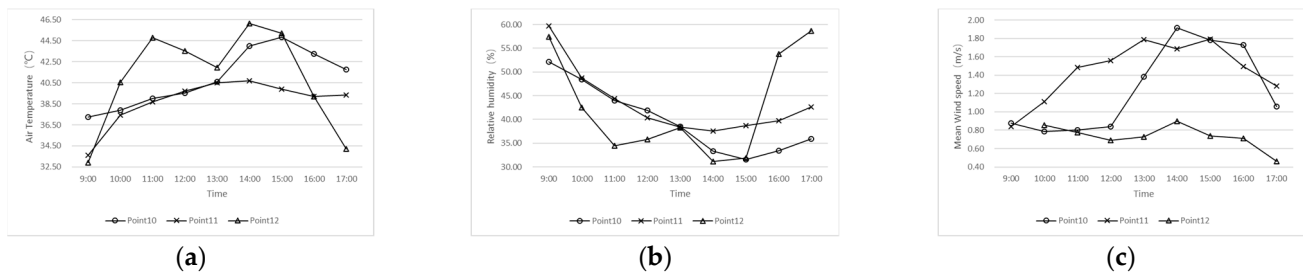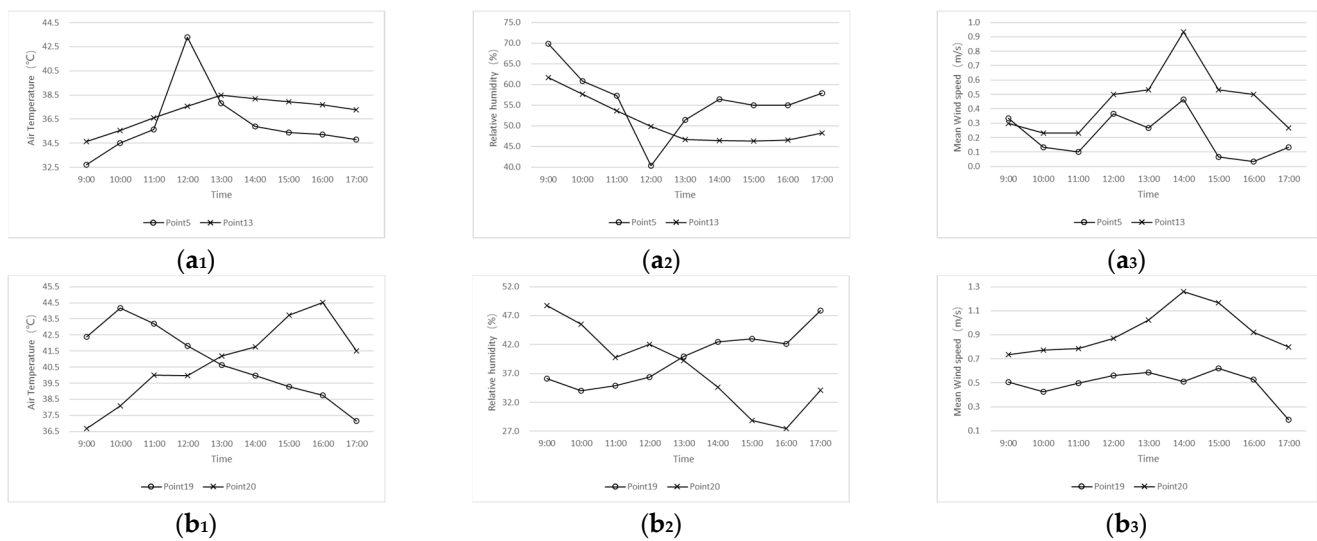
Figure 7. Comparison of points parameters. (**a**) Temperature comparison; (**b**) Relative humidity comparison; (**c**) Wind speed comparison.

The analysis of the thermal environments of the three city parks showed that large areas of vegetation and water could play significant roles in cooling. When solar radiation was strong, the cooling effects of the vegetation were stronger than those of the water bodies. The maximum temperature difference between the types of cooling was 6.1 °C. When the solar radiation weakened, the water bodies provided higher cooling rates and lower ambient air temperatures. At places with strong solar radiation, the combination of lush trees and water bodies provided good thermal environments with stable air temperatures. Although ventilation had cooling effects, it could not offset the effects of thermal radiation.

3.3. Characteristics of Thermal Environments of Commercial Streets

Figure 8a–b shows Point 5 (B-MHH) on hard pavement in the middle of a commercial pedestrian street surrounded by multistory buildings. The spaces between the buildings were moderate. The average street aspect ratio was less than 1. Point 13 (B-MHM) was located beside the commercial street outside a multistory construction, where the spaces between the buildings were small. The construction's shadow completely covered the measurement point. The average street aspect ratio was about 2. Owing to the high average street aspect ratio of Point 13, its ventilation was better than that of Point 5, which had a lower building density and higher greening rate as a result of its low average street aspect ratio. The vegetation was better at blocking solar radiation and providing stronger transpiration. According to the analysis in Figure 9, the maximum difference in the hourly wind speeds of Points 13 and 5 was about 0.5 m/s. However, the wind speeds at both measurement points did not exceed 1 m/s. During the whole day, the air temperature of Point 13 was about 2 °C higher than that of Point 5. The relatively high wind speed could not improve the environment because of poor shading.
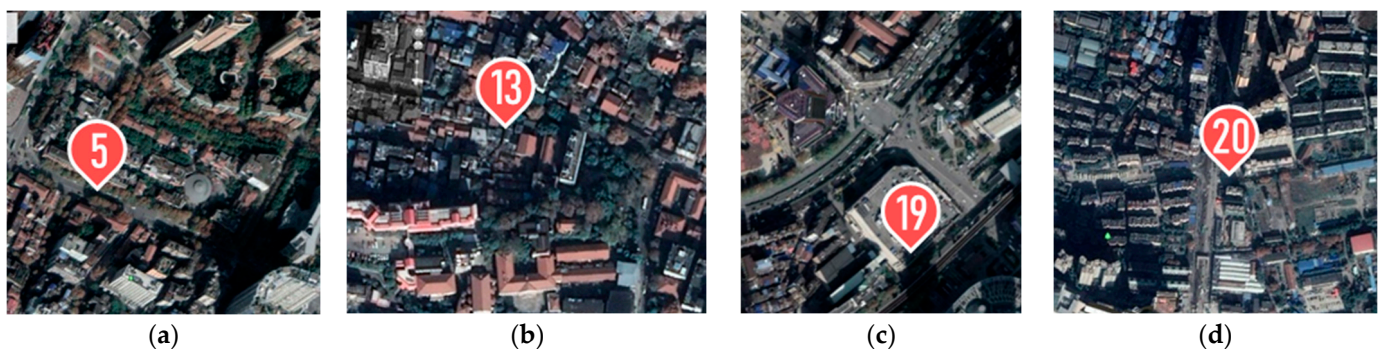
Figure 8. Satellite map of measurement points 5, point 13 and points 19–20. (**a**) Point 5; (**b**) Point 13; (**c**) Point 19; (**d**) Point 20.

Figure 9a$_1$ shows that from 11:00 to 12:00 h, Point 5 (B-MHH) was directly exposed to the sun and the temperature increased by 7.6 °C to 43.3 °C in a short time, by 5.7 °C more than that at Point 13 (B-MHM). The measurement point was under direct sunlight for a short time, so exposure to the sun was the main reason for the rise in temperature.

Figure 9. Comparison of point parameters. (a_1) Temperature comparison; (a_2) Relative humidity comparison; (a_3) Wind speed comparison; (b_1) Temperature comparison; (b_2) Relative humidity comparison; (b_3) Wind speed comparison.

The data of Point 19 and Point 20 were compared. Figure 8c,d shows that Point 19 (B-MHL) was located on a hard pavement in the southwest–northeast commercial street. The measurement point was directly exposed to the sun in the morning and covered by the shadows of the buildings in the afternoon. The buildings around this measurement point were of medium height or very high and their density was high. The greening rate around the measurement point was low with only low shrubs and small trees planted in the flower bed.

Located on the hard pavement of a commercial street running north–south, Point 20 (B-HHL) was covered by the shadows cast in the morning by the surrounding buildings of high height and density, but it was directly exposed to the sun in the afternoon. The height of the buildings around the measurement point was high and the density was also very high. There was no vegetation around the measurement point and there were only some small trees near the street.

Figure 9b_1–b_3 shows that the air temperatures of Points 19 (B-MML) and 20 (B-HHL) were above 36.5 °C on the day of the measurements, but their temperature changes displayed completely opposite trends. The temperature of Point 19 (B-MML) reached 42.4 °C at 09:00 h and was the highest (44.2 °C) at 10:00 h when the temperature difference (6.1 °C) between the points was the greatest. Afterwards, the temperature of Point 19 continued to decrease. However, at 09:00 h, Point 20 was at 36.5 °C, which was the lowest value for the whole day. Subsequently, the temperature rose steadily and reached the highest temperature (44.5 °C) at 16:00 h. The temperature changing nodes of the two measurement points were between 12:00 and 13:00 h. Solar radiation affected these two measurement points and the air temperature changed with the sun's trajectory in the sky. The maximum and minimum temperatures of the two measurement points were basically the same. The temperature difference between the lowest temperature and the highest temperature was about 6 °C and there was an opposite trend at the time of occurrence.

The shadows cast by the buildings and tall trees could provide a relatively comfortable outdoor environment during the hot summer and had better environmental effects than the good ventilation in the streets. Urban ventilation generally had low wind speed, which could not improve the thermal environment. The designs of the urban external spaces could be conducted reasonably according to the sun's movements. Outdoor activities in the morning could be arranged in a space, such as Point 20, whereas the space required for outdoor activities in the afternoon could be arranged in a space, such as Point 19. For

example, planners can locate venues for elderly people who like morning exercises within the shadows by buildings cast in the morning.

3.4. Characteristics of Thermal Environments of Campuses

Figure 10a,b shows the comparison of the areas with medium building density, such as the university campus at Point 14 (C-MMH) in the square at the entrance of the university. To the northwest of the measurement point was the main road of the city while the university's buildings lay to the northeast, east, and southwest, forming a closed layout. The buildings had an average height of about 20 m and a moderate density. There was less vegetation around the measurement point. Point 15 (C-MMH) was located on the hard-paved ground in front of the cafeteria at the center of the campus. The buildings surrounding the measurement point were mid-high rise with moderate building density and high green coverage ratio. The environments of the two measurement points were similar and mainly differed in their green coverage rates.
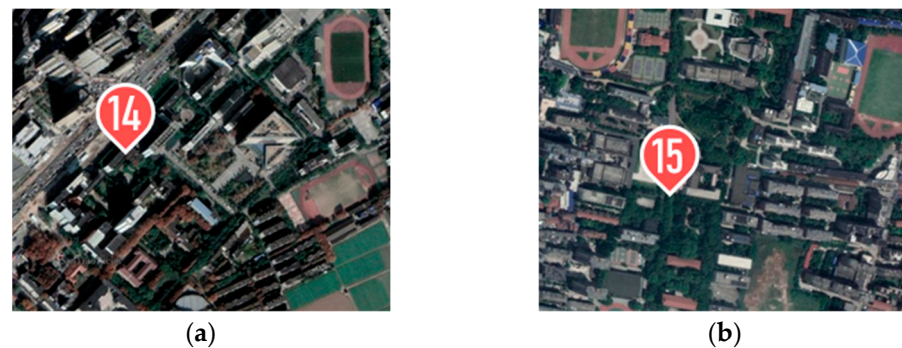
Figure 10. Satellite map of measurement points 14–15. (**a**) Point 14; (**b**) Point 15.

Figure 11a–c show that the air temperature of Point 14 was higher than that of Point 15 between 10:00 and 16:00 h while the temperature difference was between 1.2 °C and 1.9 °C. Moreover, according to the comparison of the wind speed parameters, the wind speeds at Points 14 and 15 during the whole day were small with the average wind speeds at 0.8 m/s and 0.7 m/s, respectively. At 09:00 h, the temperature of the two measurement points was the same. However, at 10:00 h, the air temperature difference between the two measurement points reached the maximum, with the temperature of Point 14 being 1.9 °C higher than that of Point 15. The vegetation and grassland around Point 15 increased the relative humidity through transpiration and played a strong role in regulating the temperature. Point 14 (C-MMH) had a very low surrounding green coverage ratio, and the solar radiant heat increased the temperature of the hard pavement. The air temperature in this Point was within 35 °C and the maximum temperature difference was 5.7 °C. However, the maximum temperature at Point 15 was 34 °C and the maximum temperature difference was 4.6 °C. Point 14 (C-MMH) had an average temperature of 1.0 °C higher than that of Point 15 (C-MMH). This difference was evidently caused by the green coverage ratio.
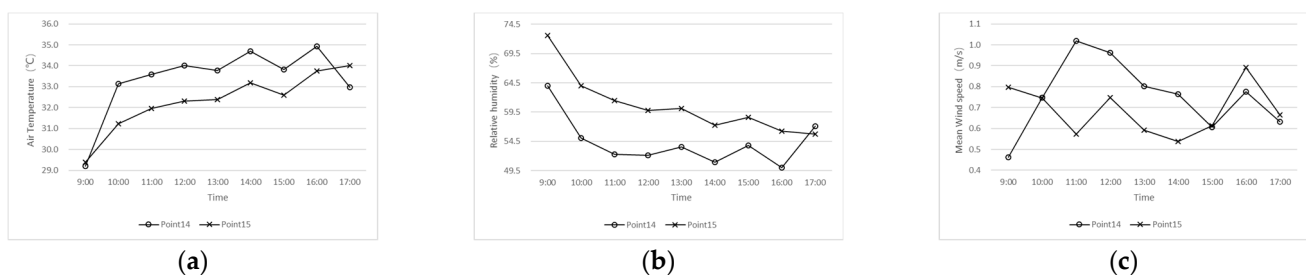
Figure 11. Comparison of measurement points parameters. (**a**) Temperature comparison; (**b**) Relative humidity comparison; (**c**) Wind speed comparison.

Although the overall building height and density were moderate and the green coverage ratio was high, the hard-paved squares on the campus still maintained high temperatures with the highest at about 1.9 °C higher and the average temperature at about 1.0 °C higher than those in the greener area of the campus in the daytime.

3.5. Comparison among Different Land-Use Types

In addition to the above analysis, it is also necessary to compare the thermal environment of urban spaces of different land use types under the same weather conditions.

(1)   Comparison of Thermal Environments of the Urban Park and Commercial Street

In Figure 12a,b, Point 4 (G1) was located on the lawn of a large park located in the central area of Wuhan City. There were many types of vegetation and the green coverage ratio was more than 85%. Point 5 (B-MHH) was located under a tree canopy on hard-paved floor in the middle of a commercial pedestrian street and surrounded by multistory buildings. The street aspect ratio was less than 1. As shown in Figure 13a, the temperature at Point 4 (G1) was higher than at Point 5 (B-MHH) during the whole day. The temperature difference was between 0.6 to 2.8 °C. The maximum temperature difference was 2.8 °C at 13:00 h and the temperature difference between the two points gradually decreased. The cooling effect of the tall tree canopy was stronger than that of grassland transpiration and the maximum temperature difference reached 2.8 °C.

Figure 12. Satellite map of measurement points 4–5. (**a**) Point 4; (**b**) Point 5.
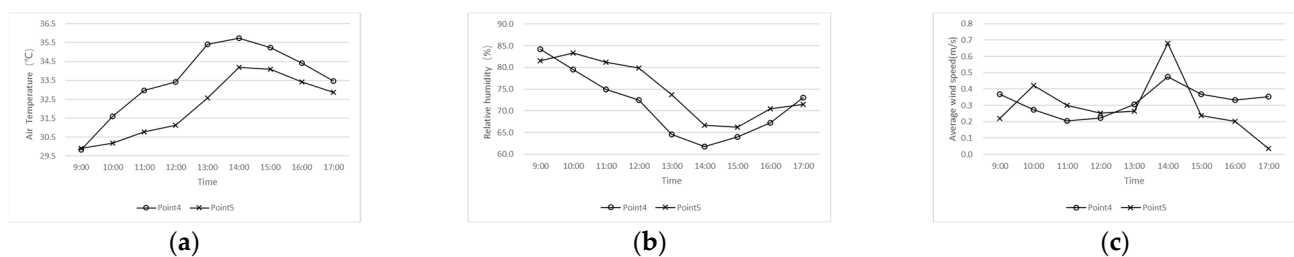
Figure 13. Comparison of point parameters. (**a**) Temperature comparison; (**b**) Relative humidity comparison; (**c**) Wind speed comparison.

(2)   Comparison of Thermal Environments of the Urban Park and Industrial Land

Urban parks and industrial lands usually have distinct thermal environment characteristics, and their comparison has research value. Figure 14a,b shows Point 6 (G2) in an open, large-scale comprehensive city square park, which had a 20,000-square-meter lawn. There were large areas of trees to the northwest and southeast of the square, as well as a circle of roadside trees along the perimeter of the square. Point 7 (M-MHL) was in an

urban industrial area whose buildings were multistory workshops, offices, and some staff dormitories with high building density and a small number of shrubs.
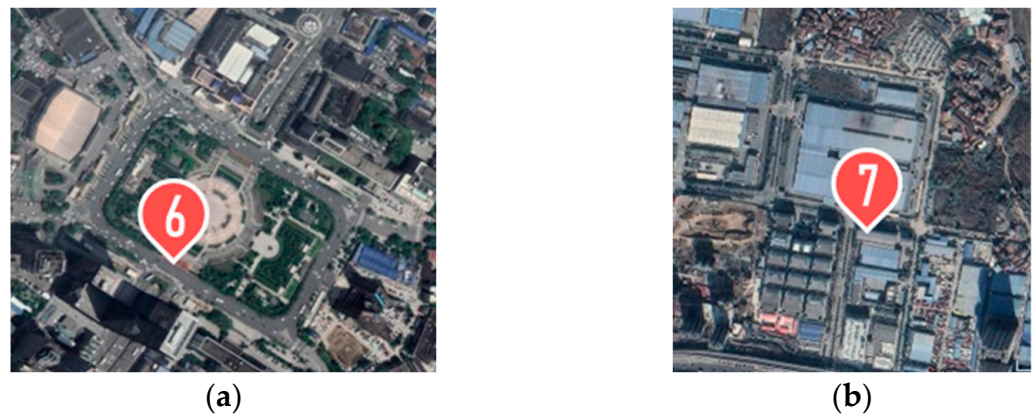
Figure 14. Satellite map of measurement points 6–7. (**a**) Point 6; (**b**) Point 7.

Figure 15a shows that the air temperature at Point 6 (G2) was lower than that of Point 7 (M-MHL) throughout the day. The temperature difference between the two points throughout was between 0.5 °C and 2.2 °C. At 14:00 h, the temperature at Point 6 was 34.3 °C and the temperature at Point 7 (M-MHL) was 36.5 °C. At this time, the temperature difference between the two points was the maximum.
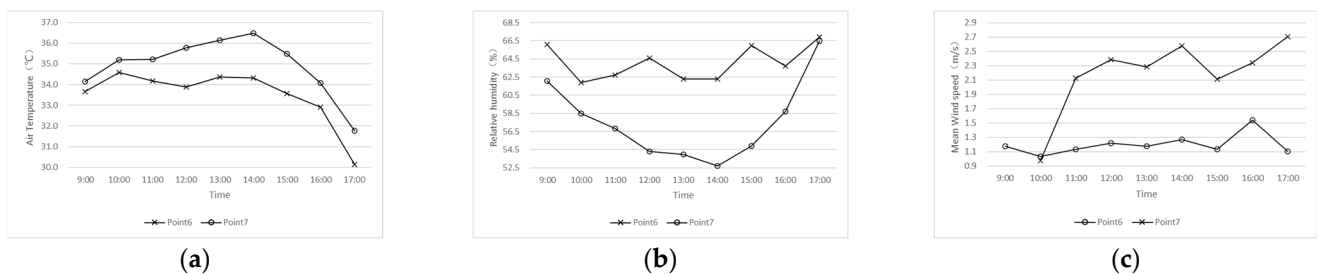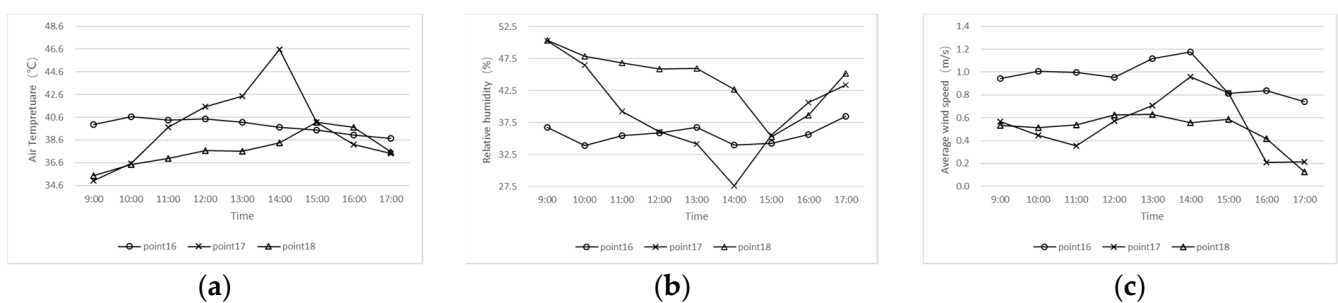

Figure 15. Comparison of point parameters. (**a**) Temperature comparison; (**b**) Relative humidity comparison; (**c**) Wind speed comparison.

Figure 15c shows that the wind speed at Point 7 (M-MHL) was higher than that at Point 6 (G2). The average wind speeds of the two points were 2.2 m/s and 1.2 m/s, respectively. When the wind speed at Point 7 (M-MHL) was higher, the air temperature was also higher. The surrounding area was an industrial plant with a large area of impermeable paving. When solar heat radiation was strong, the relative humidity was reduced by 10% from 09:00 to 14:00 h. The cooling effect of ventilation did not offset the effect of the solar radiant heat. Therefore, the air temperature at Point 7 (M-MHL) was relatively high and remained at above 34 °C until 16:00 h. The maximum temperature was 36.5 °C.

Although Point 6 was also exposed to the sun and the wind speed was low with an average of only 1.2 m/s, the large amount of vegetation around the point maintained high humidity as a result of transpiration. The relative humidity throughout the day was more than 62%, which kept the temperature below 34.6 °C. Therefore, the cooling effects of the vegetation transpiration at these points were better than that of ventilation and the maximum temperature difference reached 2.2 °C.

It could be seen that the thermal environment of the urban park was kept more stable than that of industrial land. The changes and fluctuations at Point 6 before 16:00 h were evidently less than those at Point 7. The underlying surface, which was composed mainly of green spaces, had a relatively stable temperature and relative humidity; the air temperature fluctuation remained within 1.5 °C. The air temperature fluctuated greatly at

the corresponding hard pavement interface. When the wind speed doubled, the temperature fluctuation reached 2.5 °C and the range of the relative humidity fluctuation reached about 10%.

(3) Comparison of Thermal Environments of the Campus, Residential Area, and Medical Space

The urban spaces of the campus, residential area, and medical space are often used by the residents and their difference in thermal environment was often focused. Figure 16a–c shows Point 16 (C-MMH) in an open field on the northeast side of the front door of the university's library. The green coverage ratio around the point was high, but it was still exposed to the sun all day. Point 17 (R-LHL) was in a residential area and the surrounding buildings were multistory houses. The street aspect ratio was relatively high (height: width was about 2–3), so the point lay in the shadow of the buildings. Point 18 (H-HHM) lay in the dense shade of a tree canopy on the sidewalk outside the hospital all day.

| (a) | (b) | (c) |
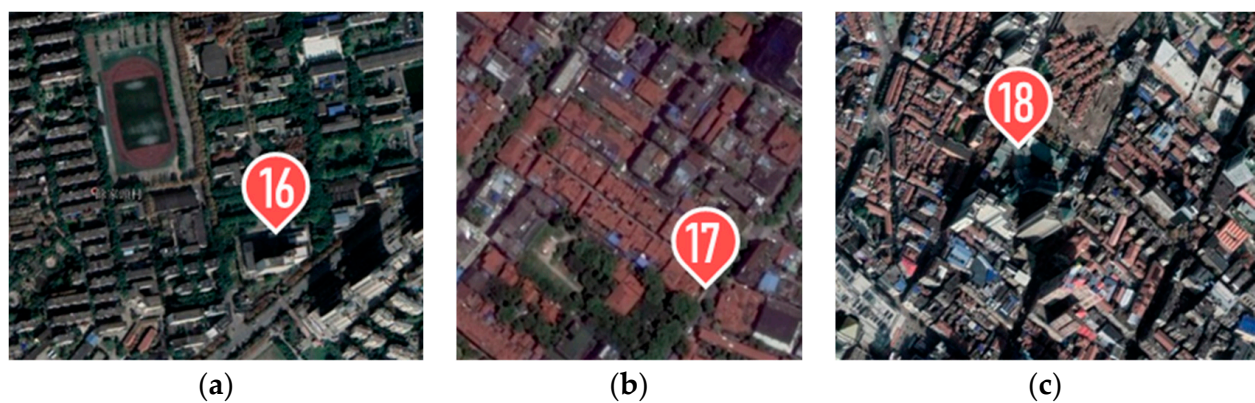
Figure 16. Satellite map of measurement points 16–18. (**a**) Point 16; (**b**) Point 17; (**c**) Point 18.

Figure 17a shows that, before 10:00 h, when solar radiation was weak, the temperature at Point 17 was approximately equal to that at Point 18. Before 10:00 h, the temperatures at Points 17 and 18 were lower by 4.5 °C and 4.3 °C, respectively, than that at Point 16. The relative humidity was 13.5% and 13.6% higher, respectively.

| (a) | (b) | (c) |

Figure 17. Comparison of point parameters. (**a**) Temperature comparison; (**b**) Relative humidity comparison; (**c**) Wind speed comparison.

According to the measurement on that day, Point 17 was in the shadow of the building because of the high street aspect ratio, Point 18 was in the shadow of the canopy of trees, and Point 16 was under direct sunlight during this period. The above analysis shows that the shadows of the trees and buildings could have cooling effects.

As can be seen from Figure 17a–c, from 11:00 to 15:00 h, the average temperature at Point 16 was 40 °C, the average relative humidity was 35.3%, and the average wind speed was 1 m/s. The average temperature at Point 17 was 42.1 °C, the average relative humidity was 34.5%, and the average wind speed was 0.7 m/s. The average temperature at Point 18 was 38.3 °C, the average relative humidity was 43.3%, and the average wind speed was

0.6 m/s. The comparisons of the values and positions of the measurement points show that Points 16 and 17 were under direct sunlight with the average temperature of Point 16 being 2.1 °C lower than that of Point 17, as a result of the cooling effects of transpiration by large areas of vegetation. The average wind speeds at Points 17 were a little higher than those of Point 18, but the relative humidity of Point 18 was 10% higher and the temperature was 4 °C lower than those of Point 17. Point 18 was in the shade of the canopy of the trees, whereas Point 17 was under direct sunlight during this period. The results indicate that the shading and transpiration of the trees increased the relative humidity, and their cooling effects were stronger than that of only ventilation. Therefore, the outdoor temperature stayed at a low level and the temperature difference reached 3 °C.

4. Discussion

The outdoor thermal environments of different types of land use were analyzed and found to be related to the building space layout, green coverage rate, and shading of each type of land use.

It was also necessary to understand the relationship in the thermal comfort indices of various land-use types in the same external space measurement environment. A significant negative correlation (R = −0.91) between the air temperature and relative humidity was found for all measurement points, which were located on different land types. However, the effects of the changes in relative humidity were small, because the air temperature decreased only by about 0.3 °C for every 1% increase. Figure 18 shows the results of the correlation analysis of the measurements of all points.
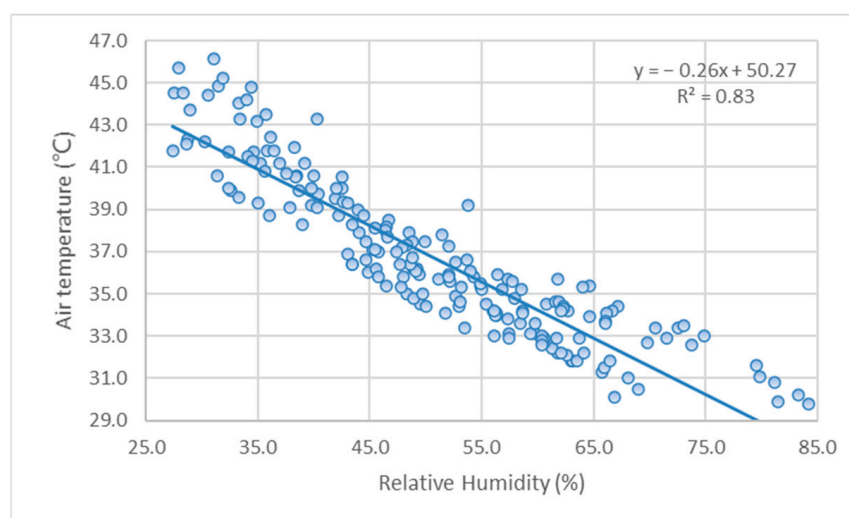
Figure 18. Scatter plot of air temperature and relative humidity.

4.1. Comprehensive Analysis Based on PET Values

The above study only investigated the individual effect of the indices of the summer microclimates, such as air temperature, relative humidity, and wind speed. PET was used to study the comprehensive relationships of the indices of microclimates. The temperature values of the black globe thermometer at the typical measurement points were added into consideration. Although PET values are expressed by temperature, they reflect the overall effects of thermal environments. Hence, they are not consistent with the data expressed only by air temperature.

On the basis of the above analysis, a statistical analysis was conducted. Correlations between PET values and temperature, relative humidity, wind speed, and black globe temperature were found, with most of the points having strong correlations. The calculation model is given in Table 3. The coefficients of these models show that air temperature had the greatest influence on the PET values of most points, followed by wind speed, which was far stronger than relative humidity, more than 10 times in many cases. However, compared

with the research of other scholars mentioned in the Introduction Section, the effects of wind speed were not obvious. It showed that the wind speed in the city was too low to play its due role.

Table 3. PET value regression analysis. Where T_a is air temperature, RH is relative humidity, V_a is wind speed, and T_g is radiant temperature obtained from the black globe thermometer.

Point	PET Value Regression Analysis
Point 14	PET was correlated with T_g and V_a at 0.05, adjusted R^2 = 0.939 PET = 2.246 T_a + 0.655 RH + 0.319 T_g + 1.893 V_a − 87.961
Point 15	PET had no correlation with V_a, adjusted R^2 = 0.854 PET = 0.252 T_a − 0.148 RH + 0.319 T_g + 34.006
Point 16	PET had no correlation with RH, PET was correlated with V_a at 0.05, adjusted R^2 = 0.99 PET = 0.739 T_a + 0.455 T_g − 0.355 V_a − 5.363
Point 17	PET was correlated with V_a at 0.05, adjusted R^2 = 1 PET = 0.810 T_a + 0.054 RH + 0.453 T_g + 0.202 V_a − 10.557
Point 18	PET had no correlation with V_a, adjusted R^2 = 0.99 PET = −0.412 T_a − 0.156 RH + 1.059 T_g + 21.790
Point 19	PET had no correlation with RH, adjusted R^2 = 1 PET = 0.607 T_a − 0.005 T_g + 0.485 V_a − 1.497
Point 20	PET had no correlation with V_a, adjusted R^2 = 1 PET = 0.711 T_a + 0.009 RH + 0.453 T_g + 0.204 V_a − 4.854

As shown in Figure 19, the PET values of Points 14 and 15 were compared. The maximum PET value at Point 14 reached 39.3 °C. From 09:00 to 10:00 h, the PET values increased by 4 °C to 36 °C and stayed at a high level. However, the PET value of Point 15 stayed at a low level at not more than 34.4 °C during the whole day. Moreover, the highest PET value appeared two hours later than that of Point 14, indicating that the PET value of Point 15 was more stable. The environmental properties of the underlying surfaces of Points 15 and 14 were similar, but the green vegetation around Point 15 was more abundant. Hence, the thermal environment was more stable and there was a lag effect on the occurrences of the poor thermal environments.
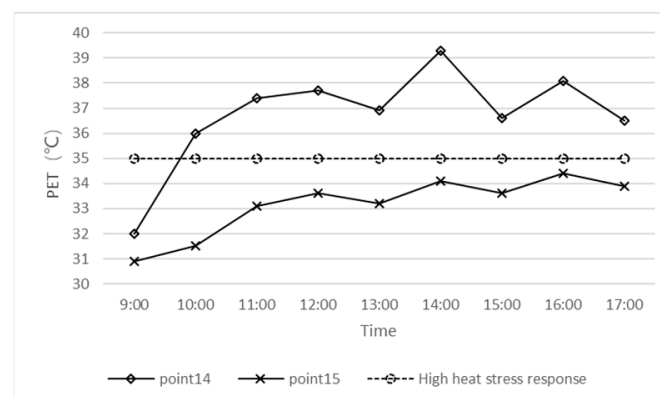
Figure 19. Comparison of PET values at measurement points 14–15.

Figure 20 shows a comparison of the PET values of Points 16, 17, and 18. The PET value of Point 16 was relatively stable, but changed rapidly in the afternoon and decreased by about 4 °C. However, the PET value of Point 16 was higher at above 45.5 °C before 15:00 h. The PET value at Point 17 changed the most throughout the day, fluctuating between 36.5 °C and 52.5 °C. The PET value of Point 18 was relatively stable with the average value at about 39.7 °C, which was 5 °C lower than that of Point 16. From the comparison of the

PET values and other meteorological parameters, it could be seen that wind speed did not have a strong influence on the overall thermal environment, whereas radiation was the most influential factor affecting PET values. The environmental PET values of tall trees were more stable than those of other green areas.
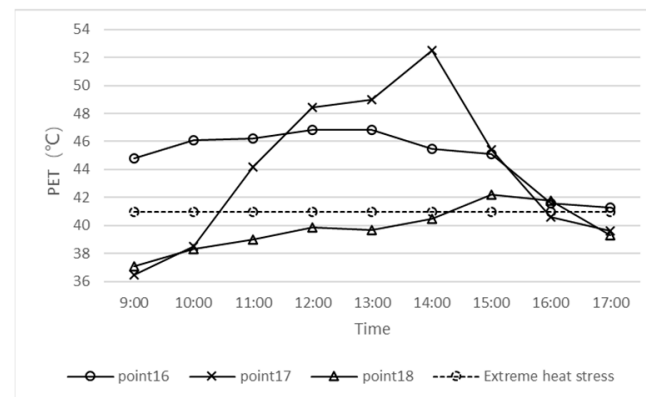
Figure 20. Comparison of PET values at measurement points 16–18.

Figure 21 shows that the PET values of Points 19 and 20 changed in the opposite direction. The PET values of the two points were relatively high with the lowest at about 39 °C and the highest at about 49.3 °C. This result was similar to that drawn from the previous diagram of air temperature. The outdoor thermal environments of commercial spaces with high density and low green rates were poor. Solar radiant heat was the main factor causing a high PET value and good ventilation could not alleviate the hot outdoor thermal environments.
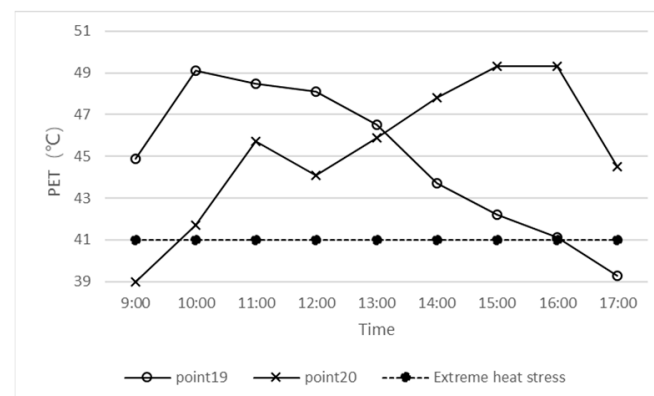
Figure 21. Comparison of PET values at measurement points 19–20.

4.2. Limitations

This study also has some limitations. Future research could start from the following three aspects. First, the outdoor spaces of different land types in built-up urban areas are complex and diverse. The types of measurement points should be more diversified to facilitate deeper comparisons and analyses. Second, this study analyzed only the characteristics of urban outdoor thermal environments during the summer. The analyses could be extended to the winter. The two-quarter improvement strategy can provide more extensive suggestions for urban planning. Third, a questionnaire survey should be used to elicit the subjective evaluation of urban residents together with the various meteorological parameters of measurement points, analyze and investigate from the perspective of urban outdoor space users, and make suggestions for improvement.

5. Conclusions

This paper presents the measurement results of the outdoor thermal environments of typical urban spaces obtained during the summer in Wuhan, China. From the results, the following conclusions were drawn.

The investigation of the outdoor thermal environments of enclosing residential buildings showed that the shade cast by the buildings reduced the air temperature efficiently. The maximum temperature difference reached 3.5 °C. In addition, the shade and transpiration of tall trees helped to keep the temperatures stable and the temperature differences within 2 °C throughout the day. For the urban parkland, when solar radiation was strong, the cooling effects of large areas of vegetation were stronger than those of water bodies. The temperature difference of these two types of underlying surfaces can reach 6.1 °C. For street valley spaces, the wind speed in the street with the aspect ratio of 2 was twice that of the street with the aspect ratio of 1, and the temperature increased by about 2 °C. With the sun's movement, the maximum temperature difference of the street space was about 6 °C without and with shading by the surrounding buildings. Campuses with surrounding vegetation had good outdoor thermal environments. The highest temperature in the square on the campus was about 1.9 °C higher than that in the green area and the average temperature in the square throughout the day was also about 1.0 °C higher.

According to the comparison of the measuring points of different underlying surfaces, the temperature of the park lawn was higher than that of the trees in the commercial street and the temperature difference reached 2.8 °C. The comparison of the green park space and the factory area showed that the temperature of the green park space was relatively high under solar radiation, but the fluctuation was small and stable. The temperature fluctuation of the factory land reached 2.5 °C and the relative humidity fluctuation was also relatively large, reaching about 10%.

From the calculation of PET, the overall effect of thermal environment can be constructed. Among the various parameters, temperature had the strongest effect on the thermal environment, followed by wind speed. The effect of relative humidity was relatively small.

From the results and information provided by this study, the thermal environment in various urban spaces was well understood. In urban planning, corresponding measures can be considered to improve the thermal comfort in various urban environments, such as shading the square area with tall trees, using the water surface to improve the areas that need to be cooled in the afternoon, effectively using the shadows of buildings to arrange citizens' activity venues and select the appropriate street aspect ratio to meet the needs of ventilation and cooling. Therefore, through the quantitative study of thermal environment, recommendations can be provided for the sustainability of climate and environment in cities, such as Wuhan, with huge urban spaces and hot summers.

Author Contributions: Conceptualization, K.L. and X.L.; methodology, K.L.; software, K.L., X.L. and K.Y.; investigation, K.L. and X.L.; resources, K.L. and X.L.; data curation, K.L. and K.Y.; writing—original draft preparation, K.L., X.L. and K.Y.; writing—review and editing, K.L. and K.Y.; visualization, K.L. and X.L.; supervision, K.L.; project administration, K.L.; funding acquisition, K.L. All authors have read and agreed to the published version of the manuscript.
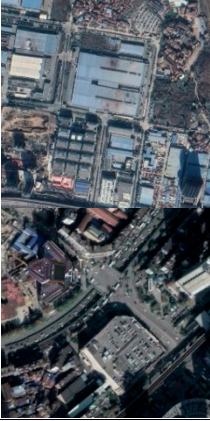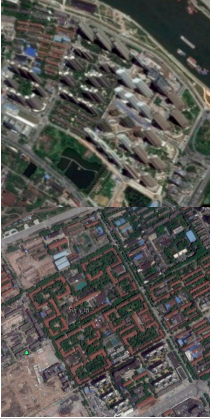
Data Availability Statement: The satellite image used in Figure 1 come from the 2.1m panchromatic image of the Resource Satellite 3. The satellite images used in Figures 4, 6, 8, 10, 12, 14 and 16 come from Google Earth. Except for the quotation noted, the measurement data and photos in this study were obtained by the corresponding author and his project team.

Appendix A

Table A1. Classification of green coverage ratio.

Level [1]	Examples	Measurement Points	Green Coverage Ratio	Characteristics
Low		Point 1, Point 3, Point 7, Point 9, Point 17, Point 19, Point 20	<30%	Land with low vegetation coverage, such as high-density residential area, pure impermeable streets, and industrial land
Medium		Point 2, Point 6, Point 8, Point 13, Point 14, Point 18	30–60%	The greening level is average, which is also combined with the land types of other functions
High		Point 4, Point 5, Point 10, Point 15, Point 11, Point 12, Point 16	>60%	Land with high vegetation coverage, such as parks

[1] In this study, the green coverage ratio was divided into three groups: low density (<30%), medium density (30–60%), and high density (>60%).

Table A2. Names, photos, building density, and 3D maps of measurement points.
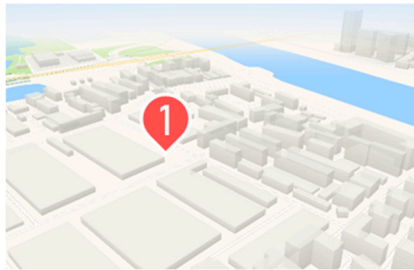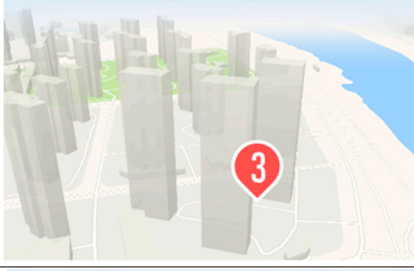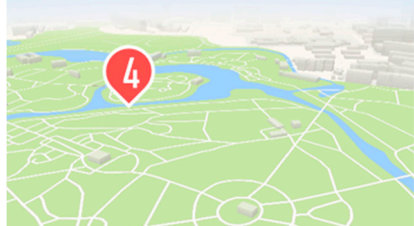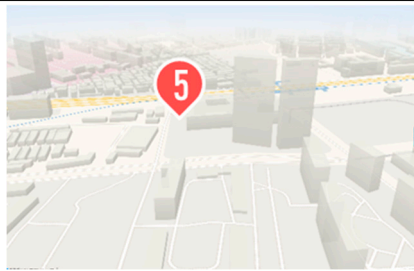
Numbers	Names	Building Density [1]	Photos	3D Maps [2]
1	Hanqi residential community	36.3% High density		
2	China Resources Central Park residential community	14.6% Low density		
3	Zhonghai Qintai Huafu residential community	13.8% Low density		
4	Jiefang Park	/		
5	Wuhan Tiandi commercial street	31.8% High density		
6	Hongshan Square	/		

Table A2. *Cont.*
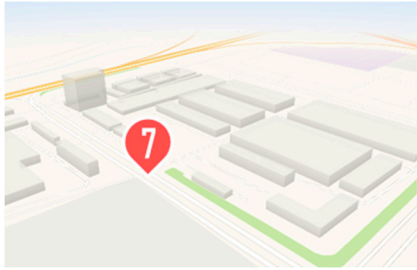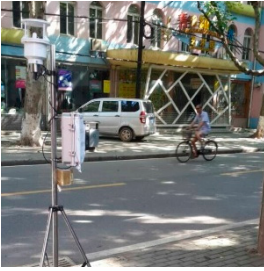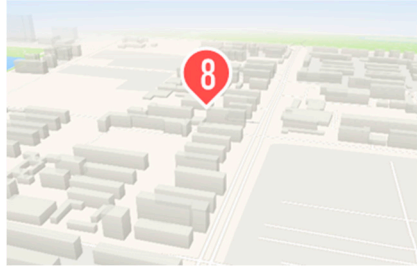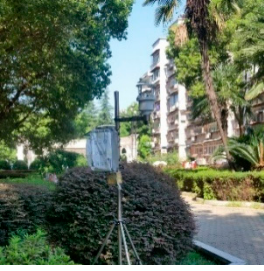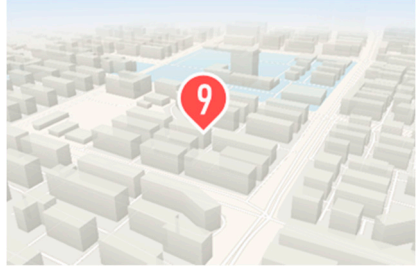
Numbers	Names	Building Density [1]	Photos	3D Maps [2]
7	SUPOR electric rice cooker company	30.4% High density		
8	Honggang 2nd Street residential community	25.7% Medium density		
9	Xinyuan residential community	35.9% High density		
10	Hongshan Park	/		
11	Zhongshan Park	/		
12	Baodao Park	/		

Table A2. *Cont.*
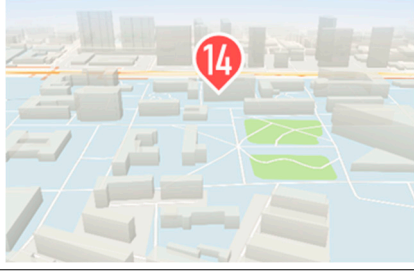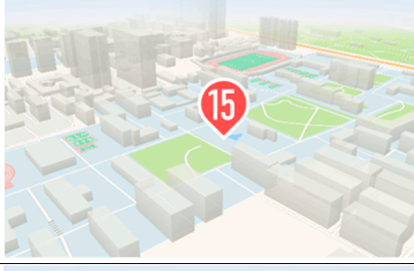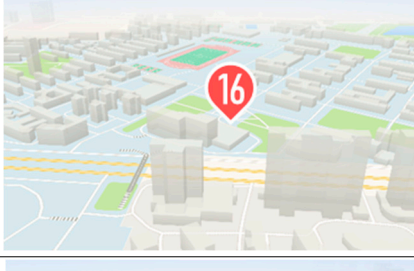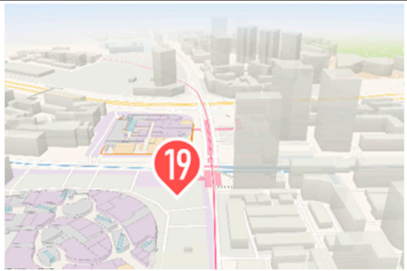
Numbers	Names	Building Density [1]	Photos	3D Maps [2]
13	Tanhualin commercial street	37.2% High density		
14	Hubei University	22.1% Medium density		
15	Central South University of Finance and Economics	16.6% Medium density		
16	Wuhan University of Technology	21.3% Medium density		
17	Tongxingli residential community	33.4% High density		
18	Wuhan Second Hospital	33.1% High density		

Table A2. *Cont.*

Numbers	Names	Building Density [1]	Photos	3D Maps [2]
19	Xunlimen commercial street	32.8% High density		
20	Lianfeng Square	36.7% High density		

[1] In this study, the building density was divided into three groups: low density (<15%), medium density (15–30%), and high density (>30%). [2] 3D graphics made with Lbs.amap.com as base.

References

1. Buettner, T. Urban estimates and projections at the United Nations: The strengths, weaknesses, and underpinnings of the world urbanization prospects. *Spat. Demogr.* **2015**, *3*, 91–108. [CrossRef]
2. McCarthy, M.P.; Best, M.J.; Betts, R.A. Climate change in cities due to global warming and urban effects. *Geophys. Res. Lett.* **2010**, *37*, L09705. [CrossRef]
3. Grimmond, S. Urbanization and global environmental change: Local effects of urban warming. *Geogr. J.* **2007**, *173*, 83–88. [CrossRef]
4. Klein, T.; Anderegg, W.R.L. A vast increase in heat exposure in the 21st century is driven by global warming and urban population growth. *Sustain. Cities Soc.* **2021**, *73*, 103098. [CrossRef]
5. Martinelli, L.; Lin, T.-P.; Matzarakis, A. Assessment of the influence of daily shadings pattern on human thermal comfort and attendance in Rome during summer period. *Build. Environ.* **2015**, *92*, 30–38. [CrossRef]
6. Santamouris, M.; Cartalis, C.; Synnefa, A.; Kolokotsa, D. On the impact of urban heat island and global warming on the power demand and electricity consumption of buildings—A review. *Energy Build.* **2015**, *98*, 119–124. [CrossRef]
7. Allegrini, J.; Dorer, V.; Carmeliet, J. Influence of the urban microclimate in street canyons on the energy demand for space cooling and heating of buildings. *Energy Build.* **2012**, *55*, 823–832. [CrossRef]
8. Song, X.M.; Zhang, J.Y.; AghaKouchak, A.; Sen Roy, S.; Xuan, Y.Q.; Wang, G.Q.; He, R.; Wang, X.; Liu, C. Rapid urbanization and changes in spatiotemporal characteristics of precipitation in Beijing metropolitan area. *J. Geophys. Res. Atmos.* **2014**, *119*, 11250–11271. [CrossRef]
9. Hondula, D.M.; Georgescu, M.; Balling, R.C., Jr. Challenges associated with projecting urbanization-induced heat-related mortality. *Sci. Total Environ.* **2014**, *490*, 538–544. [CrossRef]
10. Haines, A.; Kovats, R.S.; Campbell-Lendrum, D.; Corvalan, C. Climate change and human health: Impacts, vulnerability and public health. *Public Health* **2006**, *120*, 585–596. [CrossRef] [PubMed]
11. Sarrat, C.; Lemonsu, A.; Masson, V.; Guedalia, D. Impact of urban heat island on regional atmospheric pollution. *Atmos. Environ.* **2006**, *40*, 1743–1758. [CrossRef]
12. Mohan, M.; Sati, A.P.; Bhati, S. Urban sprawl during five decadal period over National Capital Region of India: Impact on urban heat island and thermal comfort. *Urban Clim.* **2020**, *33*, 100647. [CrossRef]
13. Deilami, K.; Kamruzzaman, M.; Liu, Y. Urban heat island effect: A systematic review of spatio-temporal factors, data, methods, and mitigation measures. *Int. J. Appl. Earth Obs. Geoinf.* **2018**, *67*, 30–42. [CrossRef]
14. Debbage, N.; Shepherd, J.M. The urban heat island effect and city contiguity. *Comput. Environ. Urban Syst.* **2015**, *54*, 181–194. [CrossRef]
15. Chen, Y.; Wang, Y.-K.; Fu, B.; Liu, Q.; Wang, S. Spatiotemporal variations of urban heat island in Chengdu city using MODIS land surface temperature data. *Resour. Environ. Yangtze Basin* **2016**, *25*, 156–162. (In Chinese)
16. Sun, R.H.; Chen, A.L.; Chen, L.D.; Lu, Y.H. Cooling effects of wetlands in an urban region: The case of Beijing. *Ecol. Indic.* **2012**, *20*, 57–64. [CrossRef]

17. Lo, C.P.; Quattrochi, D.A. Land-use and land-cover change, urban heat island phenomenon, and health implications: A remote sensing approach. *Photogramm. Eng. Remote Sens.* **2003**, *69*, 1053–1063. [CrossRef]

18. Hai, Y.; Fan, W.; Li, D. Influence of a large urban park on the local urban thermal environment. *Sci. Total Environ.* **2018**, *622*, 882–891.

19. Yang, F.; Lau, S.S.Y.; Qian, F. Urban design to lower summertime outdoor temperatures: An empirical study on high-rise housing in Shanghai. *Build. Environ.* **2011**, *46*, 769–785. [CrossRef]

20. Coutts, A.M.; White, E.C.; Tapper, N.J.; Beringer, J.; Livesley, S.J. Temperature and human thermal comfort effects of street trees across three contrasting street canyon environments. *Theor. Appl. Climatol.* **2015**, *124*, 55–68. [CrossRef]

21. Sharmin, T.; Steemers, K.; Matzarakis, A. Analysis of microclimatic diversity and outdoor thermal comfort perceptions in the tropical megacity Dhaka, Bangladesh. *Build. Environ.* **2015**, *94*, 734–750. [CrossRef]

22. Park, M.; Hagishima, A.; Tanimoto, J.; Narita, K.-i. Effect of urban vegetation on outdoor thermal environment: Field measurement at a scale model site. *Build. Environ.* **2012**, *56*, 38–46. [CrossRef]

23. Imam Syafii, N.; Ichinose, M.; Kumakura, E.; Jusuf, S.K.; Chigusa, K.; Wong, N.H. Thermal environment assessment around bodies of water in urban canyons: A scale model study. *Sustain. Cities Soc.* **2017**, *34*, 79–89. [CrossRef]

24. Du, Y.; Mak, C.M.; Huang, T.; Niu, J. Towards an integrated method to assess effects of lift-up design on outdoor thermal comfort in Hong Kong. *Build. Environ.* **2017**, *125*, 261–272. [CrossRef]

25. Janssen, W.D.; Blocken, B.; van Hooff, T. Pedestrian wind comfort around buildings: Comparison of wind comfort criteria based on whole-flow field data for a complex case study. *Build. Environ.* **2013**, *59*, 547–562. [CrossRef]

26. Liu, J.; Niu, J.; Xia, Q. Combining measured thermal parameters and simulated wind velocity to predict outdoor thermal comfort. *Build. Environ.* **2016**, *105*, 185–197. [CrossRef]

27. Ali-Toudert, F.; Mayer, H. Numerical study on the effects of aspect ratio and orientation of an urban street canyon on outdoor thermal comfort in hot and dry climate. *Build. Environ.* **2006**, *41*, 94–108. [CrossRef]

28. Dwivedi, A.; Mohan, B.K. Impact of green roof on micro climate to reduce Urban Heat Island. *Remote Sens. Appl. Soc. Environ.* **2018**, *10*, 56–69. [CrossRef]

29. Qaid, A.; Bin Lamit, H.; Ossen, D.R.; Shahminan, R.N.R. Urban heat island and thermal comfort conditions at micro-climate scale in a tropical planned city. *Energy Build.* **2016**, *133*, 577–595. [CrossRef]

30. Zhang, L.; Zhan, Q.M.; Lan, Y.L. Effects of the tree distribution and species on outdoor environment conditions in a hot summer and cold winter zone: A case study in Wuhan residential quarters. *Build. Environ.* **2018**, *130*, 27–39. [CrossRef]

31. Wuhan Municipal Statistics Bureau; State Statistical Bureau Wuhan Investigation Team. *Wuhan Statistical Year Book*; China Statistics Press: Beijing, China, 2020. (In Chinese)

32. He, Y.-h.; Chen, W.; Cai-yuan, L.; Wang, L.; Gu, Y. Climatic characteristics, causes and prediction of mid-summer high-temperature in Wuhan. *Meteorol. Sci. Technol.* **2007**, *35*, 809–813. (In Chinese)

33. Ministry of Housing and Urban- Rural Development of the People's Republic of China. *Code for Classification of Urban Land Use and Planning Standards of Development Land GB501372011*; China Architecture & Building Press: Beijing, China, 2011. (In Chinese)

34. Ministry of Housing and Urban- Rural Development of the People's Republic of China. *Standard for Urban Residential Area Planning and Design GB 50180–2018*; China Architecture & Building Press: Beijing, China, 2018. (In Chinese)

35. Li, B.; Xu, Y. Research of Wuhan modern Li-fen residential. *Huazhong Archit.* **2000**, *3*, 116–117. (In Chinese)

36. *ISO 7726:1998*; Ergonomics of the Thermal Environment—Instruments for Measuring Physical Quantities. International Organization for Standardization: Geneva, Switzerland, 1998.

37. Höppe, P. The physiological equivalent temperature–a universal index for the biometeorological assessment of the thermal environment. *Int. J. Biometeorol.* **1999**, *43*, 71–75. [CrossRef] [PubMed]

38. Frohlich, D.; Gangwisch, M.; Matzarakis, A. Effect of radiation and wind on thermal comfort in urban environments - Application of the RayMan and SkyHelios model. *Urban Clim.* **2019**, *27*, 1–7. [CrossRef]

39. Hu, H.; Xiong, Y.-J. A research summary of extreme heat wave. *Adv. Meteorol. Sci.* **2015**, *5*, 18–22. (In Chinese)